Involvement of Water Channels in Synaptic Vesicle Swelling

ALEKSANDAR JEREMIC, WON JIN CHO, AND BHANU P. JENA[1]

Department of Physiology, Wayne State University School of Medicine, Detroit, Michigan 48201

Vesicle swelling is critical for secretion; however, the underlying mechanism of synaptic vesicle (SV) swelling is unknown. A $G_{\alpha i3}$-phospholipase A2 (PLA2)–mediated involvement of the water channel aquaporin-1 (AQP1) in the regulation of secretory vesicle swelling in the exocrine pancreas has been previously reported. In the present study, the association and involvement of water channels in SV swelling was explored. Results from the study demonstrate that water channels AQP1 and AQP6, and the heterotrimeric G_o protein are associated with SVs and participate in their swelling. Exp Biol Med 230:674–680, 2005

Key words: water channels AQP1 and AQP6; synaptic vesicle swelling; photon correlation spectroscopy; atomic force microscopy

Introduction

As reported in other secretory cells (1–4), synaptic vesicle (SV) swelling is critical for secretion (5); however, the underlying mechanism of SV swelling is unknown. In mast cells, an increase in secretory vesicle volume after stimulation of secretion has been suggested from electrophysiologic measurements (6). However, a direct measurement of secretory vesicle swelling in live cells was first reported in studies on pancreatic acinar cells using atomic force microscopy (AFM; Ref. 7). Isolated zymogene granules (ZGs), the membrane-bound secretory vesicles in exocrine pancreas and parotid glands, possess Cl^-- and ATP-sensitive, K^+-selective ion channels at the vesicle membrane whose activities have been implicated in vesicle swelling (8). Additionally, secretion of ZG contents in permeabilized pancreatic acinar cells requires the presence of both K^+ and Cl^- ions. *In vitro* ZG-pancreatic plasma membrane fusion assays further demonstrate potentiation of fusion in the presence of guanosine triphosphate (GTP; Ref. 4). Analogous to the regulation of K^+ and Cl^- ion channels by $G_{\alpha i}$ at the cell plasma membrane, the regulation of K^+ and Cl^- ion channels at the ZG membrane by a $G_{\alpha i3}$ protein has been demonstrated (8). Isolated ZGs from exocrine pancreas swell rapidly in response to GTP (8). These studies suggested the involvement of rapid water entry into ZGs after exposure to GTP. When the possible involvement of water channels or aquaporins in ZG swelling was explored (9), results demonstrated the presence of aquaporin-1 (AQP1) at the ZG membranes and the participation of AQP1 in GTP-mediated vesicle water entry and swelling (9). To further understand the molecular mechanism of ZG swelling, the regulation of AQP1 in the ZG was determined (10). After immunoprecipitation with a monoclonal AQP1 antibody, detergent-solubilized ZGs co-isolate AQP1; PLA2; $G_{\alpha i3}$; the inwardly rectifying K^+ (IRK)-8 channel; and the chloride channel (ClC)-2 (10). Exposure of ZGs to either the potassium-channel blocker, glyburide; or the PLA2 inhibitor, ONO-RS-082 blocked GTP-induced ZG swelling. Red blood cells, known to possess AQP1 at the plasma membrane, also swell on exposure to the $G_{\alpha i}$-agonist mastoparan, and respond similarly to ONO-RS-082 and glyburide. Additionally, liposomes reconstituted with the AQP1 immunoisolated complex from solubilized ZGs, also swell in response to GTP. Glyburide or ONO-RS-082 abolished the GTP effect in reconstituted liposomes. Furthermore, immunoisolated-reconstituted planar lipid membranes demonstrate conductance that is sensitive to glyburide and to an AQP1-specific antibody. These results demonstrate a $G_{\alpha i3}$-PLA2–mediated pathway and potassium channel involvement in AQP1 regulation (10), contributing to our understanding of the molecular mechanism of ZG swelling. Studies in both the pancreatic acinar cell and in neurons further reveal that secretory vesicle swelling is a requirement for the regulated expulsion of intravesicular contents during secretion (5). Therefore, the present study was undertaken to understand the molecular components involved in SV swelling.

This work was supported by a grant from the National Institutes of Health NS39918 (B.P.J).

[1] To whom correspondence should be addressed at Department of Physiology, Wayne State University School of Medicine, 5245 Scott Hall, 540 E. Canfield, Detroit, MI 48201. E-mail: bjena@med.wayne.edu

The first two authors, A. Jeremic and W.J. Cho, contributed equally to this paper.

Received March 24, 2005.
Accepted June 16, 2005.

1535-3702/05/2309-0674$15.00

Results from this study demonstrate that the water channels AQP1 and AQP6, and the heterotrimeric G_o protein are associated with SVs and participate in the swelling of SVs.

Materials and Methods

Isolation of Synaptosomes, Synaptosomal Membrane (SM), and SVs. Synaptosomes, SM, and SVs were prepared from rat brains using published procedures (5, 11). Entire rat brains from Sprague-Dawley rats weighing 100–150 g were isolated and placed in an ice-cold buffered sucrose solution (5 m*M* Hepes, pH 7.4; and 0.32 *M* sucrose), supplemented with protease inhibitor cocktail (Sigma, St. Louis, MO). The brain tissue was homogenized using 8–10 strokes in a Teflon-glass homogenizer. The total homogenate was centrifuged for 3 mins at 2500 *g*, and the supernatant fraction was further centrifuged for 15 mins at 14,500 *g* to obtain a pellet. The resulting pellet was resuspended in buffered sucrose solution, and loaded onto a 3–10–23% Percoll gradient. After centrifugation at 28,000 *g* for 6 mins, the enriched synaptosomal fraction was collected at the 10–23% Percoll gradient interface. To isolate SVs and SM, isolated synaptosomes were diluted with 9 vol of ice-cold H_2O (hypotonic lyses of synaptosomes to release SVs) and immediately homogenized using three strokes in a Dounce homogenizer, followed by a 30-min incubation on ice. The homogenate was then centrifuged for 20 mins at 25,500 *g*. The resulting pellet was enriched in SM and the supernatant was enriched in SVs.

Transmission Electron Microscopy (TEM). Isolated rat brain synaptosomes and SV preparations were fixed in 2.5% buffered paraformaldehyde for 30 mins, and the pellets were embedded in Unicryl resin and sectioned at 40–70 nm. Thin sections were transferred to coated specimen TEM grids, dried in the presence of uranylacetate and methylcellulose, and examined in a transmission electron microscope.

Measurements of SV Size Using Photon-Correlation Spectroscopy (PCS) and Right-Angle Light Scattering. Changes in SV size was determined using PCS and right-angle scattering, well-known techniques for the measurement of size of submicron particles and macromolecules. Measurements using PCS were performed with a Zetasizer Nano ZS, (Malvern Instruments, Worcestershire, UK). In a typical experiment, the size distribution of isolated SVs was determined using built-in software provided by Malvern Instruments. Before determination of vesicle hydrodynamic radius, calibration of the instrument was performed using latex spheres of known size. In PCS, subtle fluctuations in the sample scattering intensity are correlated across microsecond time scales. The correlation function was calculated, from which the further diffusion coefficient was determined. Using the Stokes-Einstein equation, the hydrodynamics radius can be calculated from the diffusion coefficient (12). The intensity size distribution, which is obtained as a plot of the relative intensity of light scattered by particles in various size classes, is then calculated from the correlation function using built-in software. The particle scattering intensity is proportional to the square of the molecular weight. Volume distribution, which assigns more realistic weights to both small and big particles, is calculated from the intensity distribution using Mie theory (13, 14). Transform of the PCS intensity distribution to volume distribution is obtained using the software provided by Malvern Instruments. Measurements of SV size dynamics were determined using real-time, right-angle light scattering in a Hitachi F-2000 spectrofluorometer. Real-time scattered light intensities at 600 nm were measured as a function of vesicle radius (15). In both experimental setups, isolated SVs were suspended in isotonic buffer (0.3 *M* sucrose; 10 m*M* Hepes, pH 7.4; and 20 m*M* KCl) and changes in vesicle size monitored before and after addition of GTP or mastoparan. Values are expressed in arbitrary units and as percent light scattered over controls. Student's *t* test was performed for comparison between groups, with significance established at $P < 0.05$.

Glutamate Assay. The glutamate assay was performed using a published procedure (16). The assay relies on the conversion (reduction) of β-nicotinamide adenine dinucleotide (NAD^+) to NADH by L-glutamic dehydrogenase (GDH) in the presence of glutamate. The NADH produced fluoresces when excited with UV light, and is an indirect measurement of the glutamate content. In a typical glutamate assay, brain fractions suspended in buffered sucrose solution are supplemented with GDH (50 U/ml and 1 m*M* NAD^+). The mixture is incubated for 5 mins under continuous stirring in a thermo cuvette maintained at 37°C in a Hitachi F-2000 spectrofluorometer. Glutamate release from SV is initiated by 0.1% Triton X-100–induced SV lysis. Glutamate release is measured as an increase in fluorescence, using excitation and emission set at 340 nm and 460 nm, respectively.

Atomic Force Microscopy. Isolated SM or SVs in buffer were plated on freshly cleaved mica. Ten minutes after plating, the mica disk is placed in a fluid chamber and washed with the incubation buffer to remove unattached membrane and or SVs before imaging in the presence or absence of 20 μ*M* GTP, 100 μ*M* $HgCl_2$, 1 m*M* $CaCl_2$, and 5 m*M* EGTA. Isolated SM and SVs were imaged using the Nanoscope IIIa, an atomic force microscope from Digital Instruments (Santa Barbara, CA). All images presented in this report were obtained in the "tapping" mode in fluid, using silicon nitride tips with a spring constant of 0.06 N/m and an imaging force of less than 200 pN. Images were obtained at line frequencies of 2.523 Hz, with 512 lines per image and constant image gains. Topographical dimensions of SM and SVs were analyzed using the NANOSCOPE (R) IIIA 4.43r8 software, supplied by Digital Instruments.

Immunoblot Analysis and Glycoprotein Immunoreactivity. The total protein content in enriched SV or SM fractions was determined by the Bradford method. Sample aliquots solubilized in Laemmli sample preparation buffer were resolved using 12.5% sodium dodecyl sulfate polyacrylamide gel electrophoresis (SDS-PAGE). Resolved proteins were electrotransferred to nitrocellulose membrane for immunoblot analysis using specific antibodies to vesicle-associated membrane protein 2 (Vamp-2; Alomone Labs, Jerusalem, Israel); synaptic vesicle protein 2 (SV2), synaptophysin (Syp), and synaptotagmin 1 (Syt; gifts from R. Jahn, Yale University); $G_{\alpha o}$ (Santa Cruz Biotechnology, Santa Cruz, CA); and AQP1–9 (Aquaporins1–9 kit; α–Diagnostic, San Antonio, TX). The nitrocellulose membranes transferred by electrophoresis with the resolved SM and SV proteins were incubated for 1 hr at room temperature in blocking buffer (5% non-fat milk in phosphate-buffered saline [PBS] containing 0.1% Triton X-100 and 0.02% NaN_3), and immunoblotted for 1 hr at room temperature with the specific antibody. Primary antibodies were used at a dilution of 1:3000 (Vamp-2, SV, Syt-1, and Syp); 1:1000 (aquaporins); and 1:250 ($G_{\alpha o}$) in blocking buffer. The immunoblotted nitrocellulose sheets were washed in PBS containing 0.1% Triton X-100 and 0.02% NaN_3 and incubated for 1 hr at room temperature in horseradish peroxidase–conjugated secondary antibody at a dilution of 1:3000 in blocking buffer. The immunoblots were then washed in PBS buffer, processed for enhanced chemiluminescence (Amersham Biosciences, Piscataway, NJ) and developed using a Kodak 440 image station. Glycoproteins were visualized using florescent SYPRO Ruby and Pro-Q Emerald glycoprotein stains (Molecular Probes, Eugene, OR), according to the manufacturer's instructions.

Results and Discussion

Electron microscopy (EM; Fig. 1A and B); AFM (Fig. 1C); PCS (Fig. 1D); immunoblot analysis (Fig. 1E and F); and the assessment of glutamate content (Fig. 1G) demonstrate a highly enriched SV preparation. Synaptic vesicles in the preparations were found to have a mean diameter of 33 nm (Fig. 1C). Immunoblot analysis demonstrated that the SV preparation is enriched in Vamp2 and rab3A (Fig. 1E), both SV-specific proteins. Further immunoanalysis demonstrated the presence of several SV-specific marker proteins, such as SV2, Syt, and Syp (Fig. 1F). In addition, the isolated SVs were found to contain the neurotransmitter glutamate (Fig. 1G), which is enriched in the SV preparation. These studies collectively demonstrate the isolation of a highly enriched preparation of SVs from brain tissue for our study.

Because of the role of water channel and G_i-like proteins in swelling of secretory vesicles in the exocrine pancreas (8–10), their involvement in SV swelling was explored. When SVs were immunoprobed using water channel or aquaporin antibodies, AQP1 through AQP9, two aquaporins (AQP1 and AQP6) were found associated with SVs (Fig. 2A). However, of the two water channels present, AQP6 was enriched in SV fraction compared with the SM fraction (Fig. 2B). Our immunoblots demonstrate that besides the 28-kDa AQP1 and AQP6 forms, there is a major, approximately 40-kDa, glycosylated AQP6 form ($P < 0.05$) in SVs (Fig. 2C). This is further confirmed from the PRO-Q glycoprotein staining test, where an approximately 40-kDa glycosylated band ($P < 0.05$) is also observed. Similar to the presence of a heterotrimeric G_i-like protein in pancreatic ZG, the present study demonstrates the presence of G_o in SVs (Fig. 2C). In contrast, probing with $G_{\alpha i3}$ antibodies failed to yield any measurable signal (Fig. 2C); thus, suggesting that $G_{\alpha o}$ may be the major heterotrimeric G protein in SVs. These results further suggest that SV swelling may be similarly regulated to the ZGs in exocrine pancreas. To test this possibility, the effects on SV size of G_o protein stimulators (GTP, mastoparan), and the water channel inhibitor ($HgCl_2$), were examined using various approaches (PCS, right-angle light scattering, and AFM) to measure SV size.

Results from these studies demonstrate that SVs swell rapidly in response to GTP and mastoparan (Fig. 3). The ability of purified SVs to swell in response to GTP or mastoparan application was determined by PCS (Fig. 3A–C). Exposure of SVs to 20 μ*M* GTP or 20 μ*M* mastoparan, an amphiphilic tetradecapeptide that selectively activates $G_{i/o}$-like proteins (17), resulted in a significant increase in SV size, from 32 nm to 58 nm in mean vesicle diameter (Fig. 3A and B). The intensity distribution is also sensitive to aggregation and other vesicle-vesicle interactions in solution, which can, in some cases, dominate the distribution. Therefore, we transformed the intensity distribution to a volume distribution (Fig. 3C) to check the validity of the distribution analysis. In agreement with the determination of SV size by intensity distribution (Fig. 3A and B), determination of vesicle size by volume distribution shows similar distribution patterns of SV sizes after addition of GTP (mean diameter change from 36 to 59 nm; Fig. 3C). Because intensity and volume distributions are very similar, and the changes of mean diameter obtained by the two approaches differ by less than 5%, it is evident that vesicles undergo swelling without aggregation. The size distribution of vesicles before treatments exhibits the symmetric form of a Gaussian distribution; the distribution becomes somewhat asymmetric after swelling, indicating that not all vesicles swell to the same extent. This observation is analogous to previous observations in swelling of ZGs in live acinar cells (5). Although PCS is a valuable method for particle characterization, it is time consuming and, therefore, not appropriate for systems in which particle sizes rapidly change. To confirm the results shown in Figure 3A and B, and to assess the kinetics of SV size changes, we used right-angle light scattering with excitation set at 600 nm. It was previously shown (15) that,

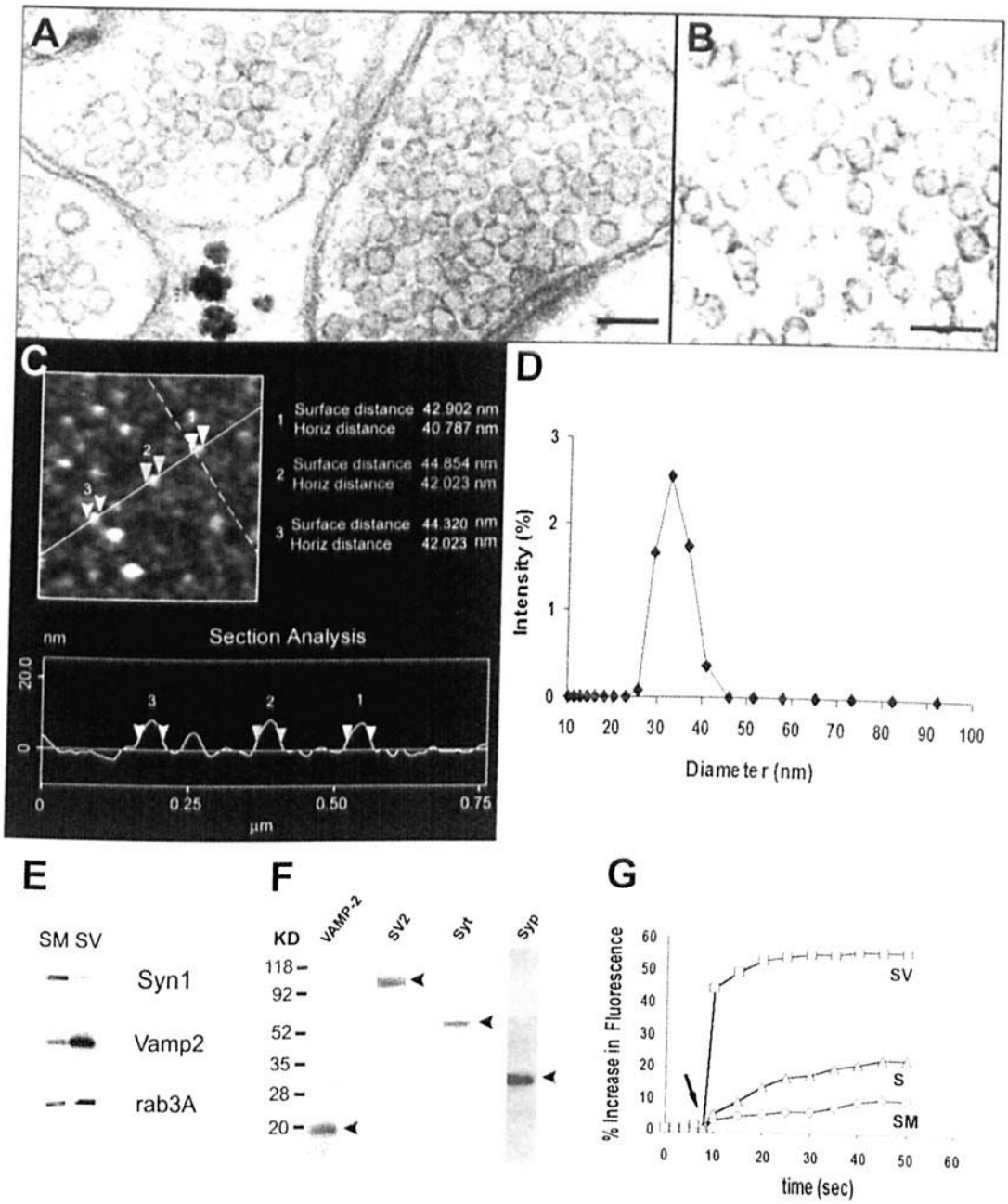

Figure 1. Isolated SVs and synaptosomes. Purity of synaptosomes (A) and SVs (B) were determined by TEM. Scale bar, 100 nm. Atomic force microscopy (C) on isolated SVs demonstrates a size distribution between 30 and 50 nm, which is further confirmed by PCS (D). Immunoblot analysis of SM and SVs demonstrates an enrichment of the SV proteins, Vamp2 and rab3A, in SVs, and the SM-associated protein, syntaxin1 (Syn1), with the SM fraction (E). Note the presence of other SV-specific proteins, such as SV2, Syt, and Syp, in the SV fraction (F). Assessment of the glutamate content per milligrams of protein in brain fractions further demonstrates enrichment in the SV pool (G).

at this wavelength, the light scattering intensity is a monotonous function of vesicle radius. Addition of 20 μM mastoparan, but not its inactive analog, mast-17, led to rapid SV swelling (Fig. 3D, inset), followed by a plateau after 50 secs (Fig. 3D). In the presence of 100 μM $HgCl_2$, however, the effect of mastoparan is suppressed. In the first 3 secs after addition of mastoparan, increase in SV swelling is a linear function of time (Fig. 3D, inset a), suggesting that influx of water and ions is unrestricted and rapid at this initial period. After this point, SV swelling slows down, and changes in SV volume takes on a logarithmic form that can be expressed by a first-order equation, with a rate constant $k = 5.4 \times 10^{-2}/s$ (Fig. 3D, inset b). Finally, after 50 secs of mastoparan exposure, SV volume attains a maximum value, when there is no further influx of solutes into the SV (Fig. 3D). The potency (Fig. 3E, inset) and efficacy of SV swelling (Fig. 3D, insets) were directly proportional to the concentration of agonist used (Fig. 3E).

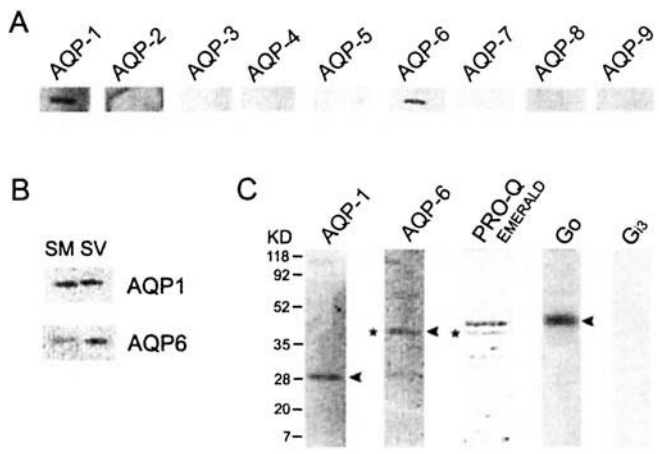

Figure 2. Association of the water channels AQP1; AQP6; and the heterotrimeric GTP-binding, G_o, with SVs. Five micrograms of isolated SVs, when resolved by SDS-PAGE and transferred by electrophoresis to a nitrocellulose membrane, demonstrate the presence of AQP1 and AQP6 after immunoblot analysis using aquaporin antibodies specific to AQP1–9 (A). Note the enrichment of AQP6 in the SV fraction (B). The approximately 28-kDa AQP1 and AQP6 proteins are present in the immunoblot, in addition to an approximately 40-kDa glycosylated form of AQP6 (C). Glycoprotein staining (PRO-Q), also demonstrates the presence of an approximately 40-kDa glycosylated band (C). Immunoblot analysis using a number of G-protein antibodies demonstrates the specific localization of the 43-kDa $G_{\alpha o}$ protein. Note the absence of $G_{\alpha i3}$ immunoreactivity.

Mastoparan-induced rapid swelling of SVs suggested the involvement of water channels, as opposed to the slow water entry by diffusion. Water channels, or aquaporins, are a family of membrane proteins that rapidly transport water across the cellular membranes (18, 19), as opposed to diffusion. Indeed, as outlined in the introduction, it has been demonstrated that, in ZGs, the membrane-bound secretory vesicles of exocrine pancreas, the AQP1 channel regulates the GTP-induced rapid gating of water (9, 10). To determine whether a similar mechanism accounts for water permeation in brain SVs, experiments using the known water channel inhibitor, $HgCl_2$, were performed. In the presence of 100 μM $HgCl_2$, the stimulatory effect of mastoparan was significantly abrogated (Fig. 3D and F), indicating a G_o-regulated, aquaporin-mediated water entry in SVs. Interestingly, with repetitive additions of mastoparan, a saturation point at a 30 μM concentration was reached (Fig. 3E), in contrast to the saturation at 50 μM with solitary mastoparan applications (Fig. 3E, inset), leading to the desensitization of SV swelling. This result clearly points to a dual, switch-on/switch-off regulation of water transport in SVs. Similar to isolated ZGs (8), Ca^{2+} has no significant effect on SV size or the extent of mastoparan-induced SV swelling (Fig. 3F).

To further assess and confirm the role of GTP on SV size, AFM studies were performed. The AFM studies (Fig. 3G) demonstrated a GTP-induced swelling of SVs. These studies, therefore, demonstrated a GTP-induced water channel–mediated (mercury-sensitive) swelling of SVs. A detail molecular pathway of ZG swelling has been elucidated (9, 10). A similar mechanism may operate in regulating SV swelling. Unlike GTP or mastoparan, Ca^{2+} had no significant effect on vesicle size or the extent of mastoparan-induced SV swelling. The lack of responsiveness of isolated SV to Ca^{2+} is similar to what has been observed previously in ZGs (8). However, Ca^{2+} was effective in regulating the size of SVs only when SVs are docked to the presynaptic membrane (5). The SVs docked to the presynaptic membrane responded to the Ca^{2+} application with a significant decrease in vesicle size, as a consequence of the expulsion of intravesicular contents (5). Recent studies demonstrate that not all secretory vesicles swell to the same extent. This is also clear from our PCS, light-scattering, and AFM results, presented in Figure 3. This differential swelling of secretory vesicles to the same stimulus may regulate the amount of expelled content (5, 20, 21) during secretion. This may explain the presence of partially empty vesicles after a secretory stimulus.

Dynamics of SV swelling may also be explained using Tanaka's theory (22), which predicts first-order kinetics for swelling of polymer networks. In our experiments, except for the first 3 secs, when the influx of water follows higher-order kinetics, swelling is strictly governed by first-order kinetics (Fig. 3D, inset b). Similar kinetics of secretory vesicle swelling is observed in goblet and mast cells (23–25), indicating that Tanaka's mechanism is widely operational in swelling and release of secretory products from various secretory cells (23–29). This mechanism assumes that intravesicular polyions form a network stabilized by small counter ions (i.e., Ca^{2+}, K^+, and H^+). The network is in the condensed state in acidic conditions. Transition to a solute state is discontinuous and reversible, and triggered by different stimuli, such as the rapid influx of water or ions (24). Phase transitions are critical phenomena that exhibit typical high cooperativity and are inherent properties of polymer networks. In the condensed state, small ions are entrapped inside a vesicular polyion network (24). After the initial rapid influx of water through aquaporins, charge compensation is lost in phase transition, because small ions, such as Ca^{2+}, are hydrated. Consequently, repulsion between polyanions increases sharply, leading to the network expansion and corresponding increase in vesicle volume. Analogous to SV swelling, work on goblet and mast cells reveal that their secretory vesicles undergo similar discontinuous and reversible volume phase transitions (24, 26). Therefore, the driving force in vesicle swelling is not simple osmotic differences across the membrane, but, rather, sudden changes in the dielectric properties of the polyionic network, which leads to the rapid release of active secretory products (27). One could expect network diffusion as the rate-determining process in SV swelling, as shown for some other secretory

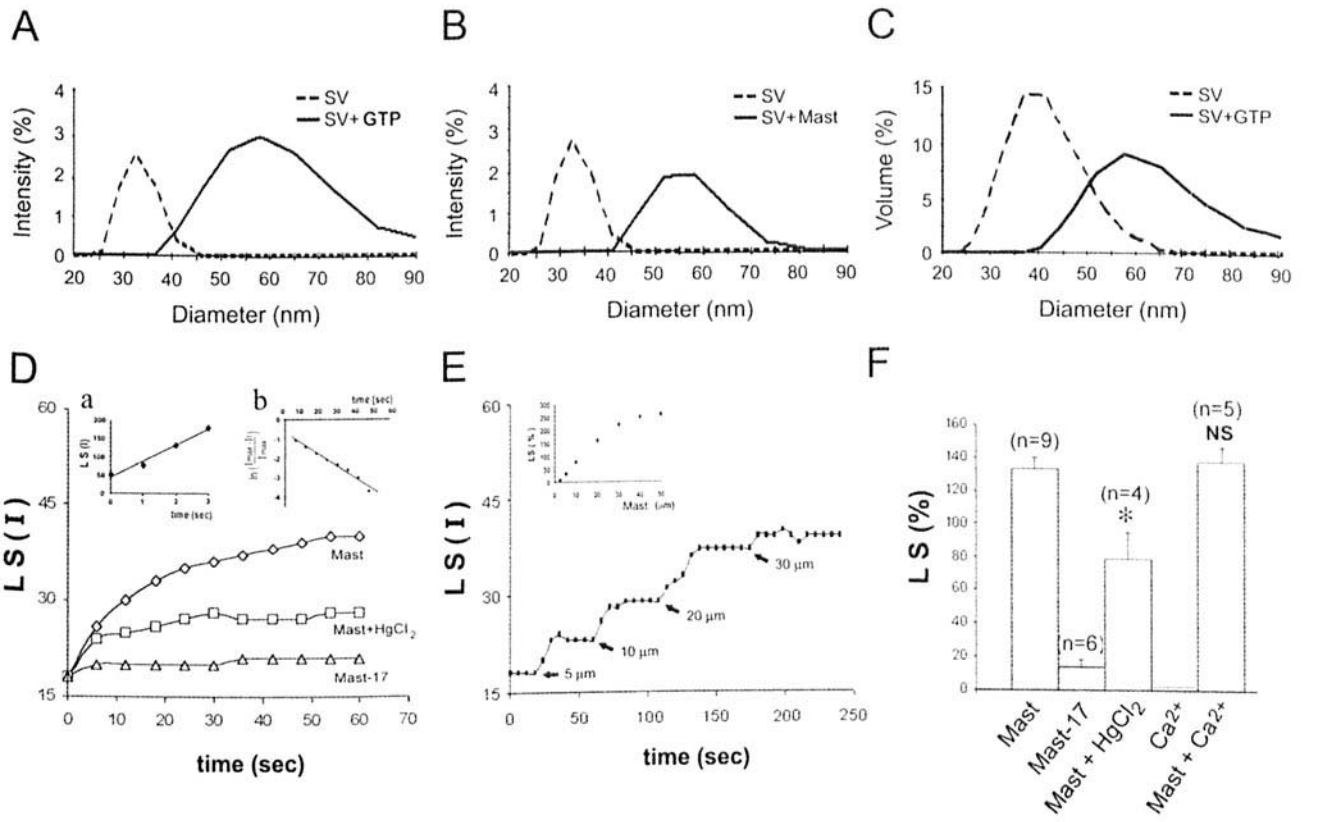

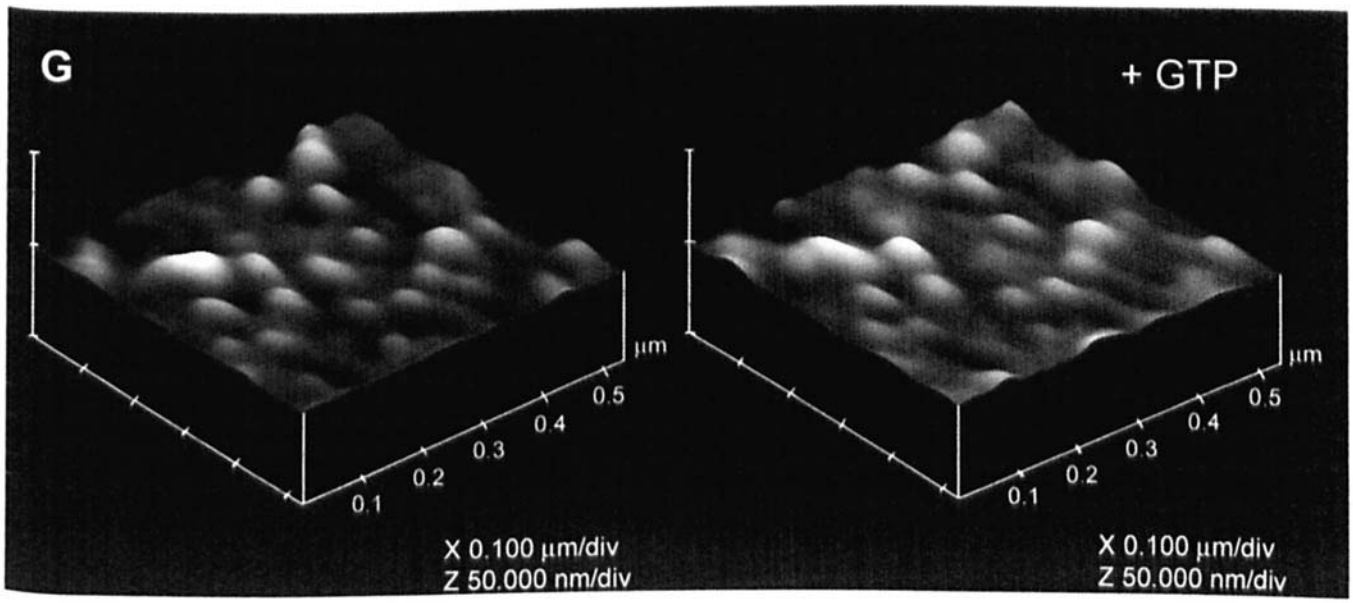

Figure 3. Guanosine triphosphate–induced swelling of isolated SVs. Isolated SVs swell in response to 20 µ*M* GTP or 20 µ*M* mastoparan (a $G_{i/o}$-agonist), as demonstrated using PCS (A–C). Similarly, right-angle light scattering also demonstrates an increase in SV size after exposure to 20 µ*M* mastoparan, an inhibition in the presence of 100 µ*M* $HgCl_2$, a water channel inhibitor, and little change in the presence of 20 µ*M* Mast-17, an inactive mastoparan peptide (D). Initial kinetics of mastoparan induced SV swelling (D, inset a). The graph depicts the first-order kinetics of SV swelling elicited by mastoparan application (D, inset b). Increase in SV swelling is directly proportional to mastoparan concentration (50 µ*M*), over the 50 µ*M* concentration, there is no further increase in size of SVs (E, inset). However, successive additions of 5, 10, 20, and 30 µ*M* mastoparan to SVs demonstrates the desensitization of SV swelling at a mastoparan concentration of approximately 35 µ*M* (E). Light scattering studies further demonstrate that mastoparan-induced SV swelling is mercury sensitive ($P < 0.05$; $n = 4$–9; Student's *t* test between Mast and Mast-$HgCl_2$ treatments), and is calcium-independent (NS, not significant; $P > 0.1$; $n = 4$; Student's *t* test between Mast and Mast-Ca^{2+} treatments). Similarly, calcium alone (2 m*M*) does not have any effect on vesicle size (F). Atomic force microscopy on isolated SVs in physiologic buffer also demonstrates an increase in SV size after exposure to 20 µ*M* GTP (G).

vesicles (24, 27). Possible phase transitions of the polyion network in product release may be reflected from studies on ZG swelling (5). Therefore, our current findings are in agreement with the universal design of secretory vesicle volume regulation, enabling the controlled release of intravesicular contents during cell secretion.

We thank Malvern Instruments for access to their Zeta Sizer.

1. Alvarez de Toledo G, Fernandez-Chacon R, Fernandez JM. Release of secretory products during transient vesicle fusion. Nature 363:554–558, 1993.
2. Curran MJ, Brodwick MS. Ionic control of the size of the vesicle matrix of beige mouse mast cells. J Gen Physiol 98:771–790, 1991.
3. Monck JR, Oberhauser AF, Alvarez de Toledo G, Fernandez JM. Is swelling of the secretory granule matrix the force that dilates the exocytotic fusion pore? Biophys J 59:39–47, 1991.
4. Sattar AKM, Boinpally R, Stromer MH, Jena BP. Gαi3 in pancreatic zymogen granule participates in vesicular fusion. J Biochemistry 131:815–820, 2002.
5. Kelly M, Cho WJ, Jeremic A, Abu-Hamdah R, Jena BP. Vesicle swelling regulates content expulsion during secretion. Cell Biol Int 28:709–716, 2004.
6. Fernandez JM, Villalon M, Verdugo P. Reversible condensation of the mast cell secretory products in vitro. Biophys J 59:1022–1027, 1991.
7. Cho S-J, Cho J, Jena BP. The number of secretory vesicles remains unchanged following exocytosis. Cell Biol Int 26:29–33, 2002.
8. Jena BP, Schneider SW, Geibel JP, Webster P, Oberleithner H, Sritharan KC. Gi regulation of secretory vesicle swelling examined by atomic force microscopy. Proc Natl Acad Sci U S A 94:13317–13322, 1997.
9. Cho SJ, Sattar AK, Jeong EH, Satchi M, Cho JA, Dash S, Mayes MS, Stromer MH, Jena BP. Aquaporin 1 regulates GTP-induced rapid gating of water in secretory vesicles. Proc Natl Acad Sci U S A 99:4720–4724, 2002.
10. Abu-Hamdah R, Cho W-J, Cho S-J, Jeremic A, Kelly M, Ilie AE, Jena BP. Regulation of the water channel aquaporin-1: isolation and reconstitution of the regulatory complex. Cell Biol Int 28:7–17, 2004.
11. Cho WJ, Jeremic A, Rognlien KT, Zhvania MG, Lazrishvili I, Tamar B, Jena BP. Structure, isolation, composition and reconstitution of the neuronal fusion pore. Cell Biol Int 28:699–708, 2004.
12. Pecora R. Dynamic Light Scattering: Applications of Photon Correlation Spectroscopy. New York: Plenum Press, 1985.
13. Mie G. Considerations on the optics of turbid media, especially colloidal metal sols. Ann Physik 4:377, 1908.
14. van de Hulst HC. Light Scattering By Small Particles. New York: Dover, 1981.
15. Matsuzaki K, Murase O, Sugishita K, Yoneyama S, Akada K, Ueaha M, Nakamura A, Kobayashi S. Optical characterization of liposomes by right angle light scattering and turbidity measurements. Biochim Biophys Acta 1467:219–226, 2000.
16. Nicholls DG, Sihra TS, Sanchez-Prieto J. Calcium-dependent and -independent release of glutamate from synaptosomes monitored by continuous fluorometry. J Neurochem 49:50–57, 1987.
17. Weingarten R, Ransnas L, Mueller H, Sklar LA, Bokoch GM. Mastoparan interacts with the carboxyl terminus of the alpha subunit of Gi. J Bio Chem 265:11044–11049, 1990.
18. Preston GM, Agre P. Molecular cloning of the red cell integral membrane protein of MW 28,000: a member of an ancient channel family. Proc Natl Acad Sci U S A 88:11110–11114, 1991.
19. Walz T, Hirai T, Murata K, Heymann JB, Mitsuoka K, Fujiyoshi Y, Smith BL, Agre P, Engel A. The three-dimensional structure of aquaporin-1. Nature 387:624–627, 1997.
20. Pothos NE, Mosharov E, Liu KP, Setlik W, Haburcak M, Baldini G, Gershon DM, Tamir H, Sulzer D. Stimulation-dependent regulation of the pH, volume and quantal size of bovine and rodent secretory vesicles. J Physiol 542:453–476, 2002.
21. Sombers LA, Hanchar HJ, Colliver TL, Wittenberg N, Cans A, Arbault S, Amatore C, Ewing AG. The effects of vesicular volume on secretion through the fusion pore in exocytotic release from PC12 cells. J Neurosci 24:303–309, 2004.
22. Tanaka T, Fillmore DJ. Kinetic of swelling of gel. J Chem Phys 70:1214–1218, 1979.
23. Tam PY, Verdugo P. Control of mucus hydration as a Donnan equilibrium process. Nature 292:340–342, 1981.
24. Verdugo P. Goblet cells secretion and mucogenesis. Ann Rev Physiol 52:157–176, 1990.
25. Zimmerberg J, Whitaker M. Calcium causes irreversible swelling of secretory granules during exocytosis. Nature 315:581–584, 1985.
26. Fernandez JM, Villalon M, Verdugo P. Reversible condensation of mast cell secretory products in vitro. Biophys J 59:1022–1027, 1991.
27. Nanavati C, Fernandez JM. The secretory granule matrix: a fast-acting smart polymer. Science 259:963–965, 1993.
28. Verdugo P. Polymer gel phase transition: a novel mechanism of product storage and release in mucin secretion. Biophys J 49:231a, 1986.
29. Verdugo P, Aitken M, Langley L, Villalon MJ. Molecular mechanism of product storage and release in mucin secretion. II. The role of extracellular Ca^{2+}. Biorheology 24:625–633, 1987.